2023 IEEE 26th International Conference on
Intelligent Transportation Systems (ITSC)
24-28 September 2023. Bilbao, Bizkaia, Spain

Modeling car-following behavior of electric adaptive cruise control vehicles using experimental testbed data

Arian Zare, Mingfeng Shang, *Student Member, IEEE*, Xingan (David) Kan, and Raphael Stern, *Member, IEEE*

***Abstract*— Automated vehicles (AVs) have the potential to revolutionize the transportation industry. While extensive research has been conducted to explore the benefits of AVs on traffic flow, commercially available adaptive cruise control (ACC) vehicles with advanced driver assistance features have been shown adverse effects on traffic flow. As vehicle automation advances, electric vehicles (EVs) equipped with ACC are emerging as an alternative to traditional internal combustion engine (ICE) vehicles. However, there is still a limited understanding of the differences in vehicle dynamics between EV-ACC and ICE-ACC vehicles.**

This study utilizes microscopic car-following models to describe the vehicle dynamics of EV-ACC vehicles. The model parameters are calibrated based on an experiment conducted with commercially available EV-ACC vehicles. The calibration results indicate that the optimal velocity relative velocity (OVRV) model outperforms the intelligent driver model (IDM) in most gap settings by up to 37%, suggesting that the OVRV model can effectively capture the driving behavior of EV-ACC vehicles. However, simulations of a string of vehicles imply that the IDM is more accurate in capturing amplifications due to velocity disturbances. Therefore, the development of higher-fidelity microscopic car-following models specifically for EV-ACC vehicles is necessary.

I. Introduction

The emergence of automated vehicles (AVs) has the potential to revolutionize the transportation landscape. The behavior of AVs at the microscopic level significantly impacts macroscopic traffic dynamics. Previous studies have employed traffic simulations to evaluate the effects of both fully automated vehicles (e.g., SAE Level 5) and partially automated vehicles with driver-assist enabled features [1]–[3]. In recent decades, advanced driver assistance (ADAS) features such as adaptive cruise control (ACC) (e.g., SAE Level 1-2) have become commercially available, with the majority of vehicles now offering this technology. While fully automated vehicles have offered multiple benefits on traffic flow, e.g., string stable traffic flow [4], higher highway throughput [2], lower fuel consumption and emissions [5], recent studies have found that these benefits are likely not been shown on commercially available ACC vehicles. Specifically, Shang and Stern [3] investigate the impacts of commercially available ACC vehicles on traffic flow and find that they may reduce highway throughput.

A. Zare, M. Shang, and R. Stern are with the Department of Civil, Environmental, and Geo-Engineering at the University of Minnesota, MN 55455, USA (email: {zare0032, shang140, rstern}@umn.edu).

X. D. Kan is with the Department of Civil, Environmental, and Geomatics Engineering at Florida Atlantic University, FL 33431, USA (email: kanx@fau.edu).

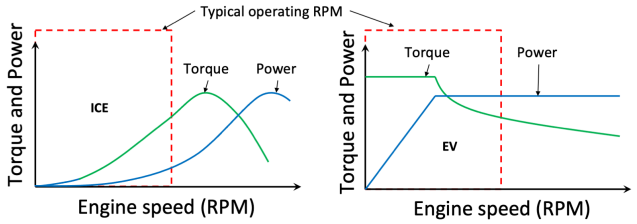

Fig. 1: Illustrative plots showing approximate side-by-side comparison of torque and power generation for ICE vehicles and EVs showing that EVs can provide maximum power under typical driving conditions.

In parallel to advancements in vehicle automation, vehicle electrification is another disruptive development in the automotive industry. Increasingly, electric vehicles (EVs) are becoming viable as an alternative to internal combustion engine (ICE) vehicles. Many of these electric vehicles come equipped with driver assist features such as ACC.

While many aspects of EVs are similar to ICE vehicles, they have some key mechanical differences, making their vehicle-level dynamics distinct. Specifically, as engine speed (revolutions per minute) increases, an internal combustion engine gradually increases torque output. This higher engine speed is necessary to achieve high power output on an ICE vehicle, since power is the product of engine speed and torque. In most driving scenarios, people drive at moderate engine speeds (3,000 revolutions per minute maximum in most situations) to achieve fuel-efficient driving, as shown in Fig. 1. This is also true for most ACC controllers, which generally rely on low engine speeds for most of the driving to reduce fuel consumption. As a result, ACC vehicles generally are unable to utilize the full power capabilities of the ICE vehicles they are controlling.

In contrast, electric motors, which power EVs, are capable of producing high initial torque at low revolutions as shown in Fig. 1. Thus, EVs are able to provide higher acceleration under typical driving conditions, making EV-ACC vehicles more reactive to changes in the traffic conditions around them. Additionally, EVs utilize regenerative braking, which allows for stronger braking capabilities without delay. As a result, EV-ACC vehicles can potentially drive with shorter inter-vehicle spacing and accelerate faster than ICE-ACC vehicles, even in oscillatory traffic conditions.

Microscopic car-following models can describe a vehicle driving behavior with an ordinary differential equation (ODE), and can be used for examining traffic flow impacts through simulations [6]. Since the 1960s [7], the develop-

ment of numerous microscopic car-following models has focused on accurately describing different aspects of traffic flow including the development of stop-and-go waves [8], and collision-free driving [9], among other features.

Calibrated car-following models have shown to be a useful tool in assessing the impacts of ICE-ACC vehicles via microscopic simulations [2]–[4], [10]–[12]. Similarly, these calibration approaches may also be extended to EV-ACC vehicles with EV-ACC data collected in field experiments.

While considerable research has modeled ICE-ACC dynamics and validated the widely-used microscopic car-following models [12]–[14], it is still unclear if those models have capabilities to capture the EV-ACC driving behavior seen in mass-market vehicles as well.

To this end, we highlight the contributions of this study as follows:

- We analyze the collected EV-ACC car-following field experiment data and use it to calibrate commonly-used ACC car-following models.
- We present calibrated model parameter values that may contribute to the transportation community for future use in the simulation-based studies.
- We have also conducted simulation analyses to estimate traffic wave amplification with EV-ACC vehicles, and compare this to ICE-ACC vehicles.

The remainder of this article is outlined as follows. In Section II, the EV car following data are introduced and analyzed. We present mathematical models for modeling EV-ACC vehicle dynamics in Section III. In Section IV, we review the calibration process and simulation approach in this study. In Section V, numerical analyses are conducted to validate the performance of microscopic car-following models calibrated with the EV-ACC data. This article is concluded in Section VI with a future study direction.

II. EV CAR FOLLOWING DATA

To understand and model EV-ACC vehicle dynamics at the microscopic (following setting) level, we use experimentally collected trajectory data collected from a commercially-available EV-ACC vehicle. The EV-ACC data used for model calibration is collected by co-author Kan as part of an extensive data collection campaign. More details on the full data collection protocol are available in [15], [16], and a brief description of the data collection is provided next for completeness.

Car following experiments are conducted in a controlled setting using an (ICE) lead vehicle that drives a pre-determined speed profile under human control, and an EV-ACC vehicle that follows the lead vehicle with ACC engaged. The lead vehicle used in the experiments is a 2021 Toyota Camry with a 3,310 lb curb weight and maximum power output of 203 horsepower at 6,600 rpm from a 2.5-liter naturally aspirated engine. The following vehicle (the EV-ACC subject vehicle used in this study) is a 2022 Hyundai IONIQ 5 with a 4,414 lb curb weight and 225 hp, 258 ft-lb electric motor. Both the ICE lead vehicle and EV-ACC following (subject) vehicle are shown in Figure 2. The

Fig. 2: ICE lead vehicle (left) and EV-ACC test vehicle (right) used for data collection experiments.

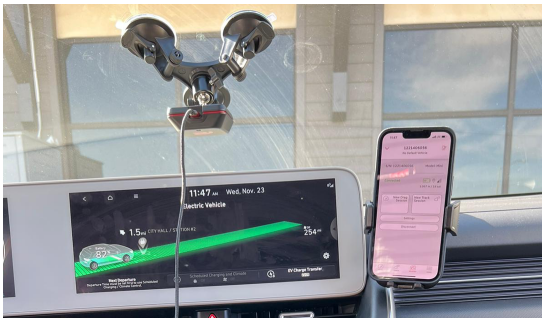

Fig. 3: Data collection setup mounted on vehicle windshield with Racebox GPS receiver and data logging on the dashboard-mounted smartphone.

Hyundai IONIQ 5 was selected based on its availability as a widely sold electric vehicle from a reputable manufacturer. Moreover, the weight to peak power ratio of this vehicle is comparable to that of many commonly sold traditional gas-powered vehicles. While it is likely that the results found for the IONIQ 5 will hold for other EVs, further data collection is needed to confirm this.

In each car following experiment, the position of both the lead vehicle and (EV-ACC) following vehicle was recorded using a Racebox GPS logger, which is capable of recording data at up to 25 Hz with a horizontal accuracy of 10 cm. The individual vehicle position is then used to compute the inter-vehicle spacing via the Haversine distance formula. The data collection setup, including the Racebox GPS receiver and smartphone used for data collection are shown in Figure 3.

During each experiment, both vehicles start with an initial distance, and then accelerate (under human control) to a pre-defined speed. After reaching the pre-defined free-flow speed, the driver of the EV-ACC following vehicle activated the ACC feature and manually accelerated slightly above the setpoint speed to ensure the vehicles reached the equilibrium (ACC) spacing. This stabilization process is intended to mimic the equilibrium flow conditions at capacity when vehicles are driven sufficiently close for ACC to be engaged.

Once an equilibrium steady-state flow was achieved, the driver of the lead vehicle manually decelerated to a lower congested speed, and remained at that speed for 10 seconds before returning to the free-flow speed.

In total, four different free-flow speeds were tested: 97 km/hr (60 mph), 89 km/hr (55 mph), 72 km/hr (45 mph), and 56 km/hr (35 mph). For each of these free-flow speeds, 3 to 4 congested speeds were tested. An example of one

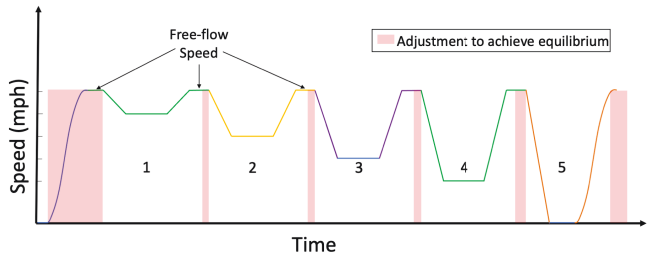

Fig. 4: Sample lead vehicle pre-determined speed profile with one free-flow speed and five different congested speeds. Note the shaded red area represents times at which the EV-ACC vehicle is reaching a free-flow equilibrium before the next congested speed is tested.

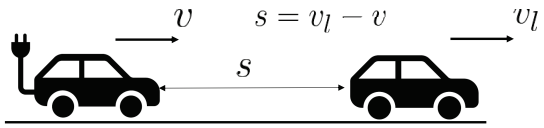

Fig. 5: General car following setup showing lead vehicle being followed by an (electric) vehicle.

speed profile for the lead vehicle, with five different congested speeds, is shown in Figure 4. Each series of speed fluctuations were repeated 8 times, with two repetitions for each possible space-gap setting (short gap, medium gap, long gap, and extra-long gap). This resulted in a total of 136 speed fluctuations in the dataset.

III. Modeling Car-Following Dynamics

In this section, we present the car-following models that will be calibrated using the collected EV-ACC data.

A. Generic function

Car following models also referred to as microscopic models, are often used to describe the driving dynamics of individual vehicles. The general concept of car-following models dates back to the 1960s [17], and is based on the idea that the acceleration (or speed) of a particular vehicle is based on the behavior of the vehicle in front of it (also referred to as the lead vehicle). Specifically, as shown in Figure 5 and the generic car following model form presented in (1), the following vehicle acceleration $a(t)$ at time t is a function of the inter-vehicle spacing $s(t)$ at time t, the following vehicle speed $v(t)$, at time t, and the relative speed with respect to the lead vehicle $\dot{s}(t) = v_\ell(t) - v(t)$, at time t, with lead vehicle speed $v_\ell(t)$. For simplicity of notation, the time index is often omitted.

$$a(t) = f(s(t), v(t), \dot{s}(t)), \tag{1}$$

The functional form in (1) can describe a wide range of previously introduced car-following models. For a summary of different car following models, the interested reader is referred to [18].

B. OVRV

Inspired by the constant time gap (CTH) ACC control policy [19], [20] often used in the design of ICE-ACC vehicles, the optimal velocity, relative velocity (OVRV) car following model has been widely used to model ICE-ACC vehicle dynamics, and has been shown to accurately describe their car following behavior [11], [21], [22]. The model combines a constant time gap policy with a relaxation to the lead vehicle speed:

$$a(t) = k_1 \left(s - \eta - \tau v\right) + k_2(v_l - v), \tag{2}$$

where model parameter values $\boldsymbol{\theta}_{\text{OVRV}} = [k_1, k_2, \eta, \tau]^\top$ can be adjusted to match a specific following vehicle's driving dynamics. Notably, k_1 and k_2 are velocity gain and velocity difference gain, respectively. Parameter τ is the time headway, and η represents the stopping distance.

C. IDM

Another commonly used car following model for describing both human drivers and ICE-ACC vehicles is the intelligent driver model (IDM) [9]. The IDM is capable of describing both symmetric car-following behavior, where acceleration and braking are the same, as well as an asymmetric car-following behavior, where braking and acceleration differ. Moreover, the IDM has been extensively used to describe ICE-ACC dynamics with high accuracy [12], [23].

The IDM takes the form:

$$a(t) = \alpha \left(1 - \left(\frac{v}{v_0}\right)^{\delta} - \left(\frac{\hat{s}(v, \dot{s})}{s}\right)^2\right) \tag{3}$$

$$\hat{s}(v, \dot{s}) = s_0 + \tau v - \frac{v\dot{s}}{2\sqrt{\alpha\beta}} \tag{4}$$

where model parameter values $\boldsymbol{\theta}_{\text{IDM}} = [v_0, \tau, \delta, s_0, \alpha, \beta]^\top$ are subjected to calibrate for a specific car-following profile. Of note, $\boldsymbol{\theta}_{\text{IDM}}$ can be physically interpreted: v_0 is the desired speed that a vehicle may drive; τ is the time headway; δ is an acceleration exponent; s_0 is the stopping distance; α and β are maximum acceleration and comfortable braking rate, respectively.

IV. Calibration and Simulation

In this section, we review the calibration process and the simulation approach to obtain the vehicle dynamics.

A. Calibration approach

The objective of model calibration is to obtain the best-fit $\boldsymbol{\theta}$ by minimizing the error between the simulated trajectories and experimental data such that the simulated dynamics are close to the experimental data as much as possible. While many approaches to obtain the best-fit parameter values are available [24], the batch optimization approach is commonly used in the transportation community [12], [14], [23].

With the experimentally collected leader-follower trajectory data presented in Section II, we minimize the spacing *root mean square error* (RMSE) between the simulated trajectory and the experimental data. Notably, reducing the spacing RMSE will simultaneously reduce the velocity error due to the inherently spacing-velocity relationship [23]. Therefore, the spacing RMSE is given as

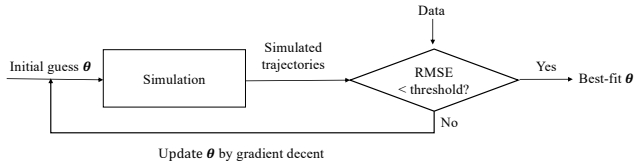

Fig. 6: Batch calibration approach where a simulation, using the current candidate parameter values, is used to compute the RMSE, and the parameter values are updated via gradient descent until simulated trajectories are sufficiently similar to observed experimental trajectory data.

$$\begin{aligned} \underset{s,v,\boldsymbol{\theta}}{\text{minimize}}: \quad & \text{RMSE} = \sqrt{\tfrac{1}{\mathcal{T}}\textstyle\sum_0^{\mathcal{T}} (s_{\text{m}}(t) - s(t))^2} \\ \text{subject to:} \quad & a(t) = f(\boldsymbol{\theta}, s, v, \dot{s}), \\ & \dot{s}(t) = v_{\ell,\text{m}}(t) - v(t), \\ & s(0) = s_{\text{m}}(0), \\ & v(0) = v_{\text{m}}(0), \\ & \boldsymbol{\theta} \in \boldsymbol{\theta}_c, \end{aligned} \tag{5}$$

where $\mathcal{T}$ denotes the final time stamp of the training period, the subscript m denotes the simulated trajectory, the subscript l denotes the lead vehicle profile, $s(0)$ and $v(0)$ are the initial spacing and speed, respectively. Of note, we rewrite $a(t)$ defined in (1) for the variation of $\boldsymbol{\theta}$ which holds physical bounds in $\boldsymbol{\theta}_c$.

The batch calibration process is illustrated in Fig. 6. Initially, an initial guess for the parameter values are input into the calibration. Then, we obtain the simulated trajectories using the current candidate parameter values. When comparing the simulated trajectories and the experimental data, we calculate the spacing RMSE with (5). Finally, to obtain the best-fit model parameter values, the current parameter values are updated via gradient descent until simulated trajectories are sufficiently similar to the observed experimental trajectory data. The calibration process was carried out with the package of `scipy.optimize.minimize` in Python.

B. Simulation approach

The simulation process is adopted from Euler's method which indicates the continuous time model can be discretized into time steps Δt:

$$\begin{bmatrix} s \\ v \end{bmatrix}_{t+\Delta t} = \begin{bmatrix} s \\ v \end{bmatrix}_t + \begin{bmatrix} \dot{s} \\ a \end{bmatrix}_t \Delta t, \tag{6}$$

where s, v, a, and $\dot{s}$ are defined above.

V. Model validation and comparison

In this section, we begin by presenting the calibration results as well as the parameter values for the IDM and OVRV models obtained by simulation on the experimental trajectory data. To compare the performance of each model under different spacing settings numerically, we calculate the spacing RMSE for each scenario. Then, the results are validated by showing the simulated spacing and speed for the medium and long settings. Moreover, the amplification analysis and comparisons are conducted on the calibrated models using a simulated string of vehicles that behave based on the parameter values of the IDM and OVRV models.

A. Calibration results

As introduced in Section II, model Parameter values of the IDM and OVRV model are calibrated for four different gap settings: 'short', 'medium', 'long', and 'xlong' (i.e., extra-long). The RMSE values are calculated by (5) using the collected data and the simulated trajectories. We present model parameter values and the RMSE for each model under different gap settings in Table I.

To obtain the best-fit model parameter values for EV-ACC vehicles, we slice the data into six subsets used for training purposes. Each training dataset is 200 s long for each gap setting. To avoid data overfitting, we calibrate each model on the shorter training set and test model performance on the entire dataset. The model parameter values listed in Table I are calibrated from the training set with the lowest spacing RMSE.

To validate the parameter values for the IDM and OVRV model, speed and spacing are reproduced using the best-fit parameter values for each gap setting. Fig. 7 and 8 show the simulated trajectories and the experimental trajectories for the medium and long gap settings. Numerically, the comparisons of the RMSE between different settings show that the OVRV model has better performance than the IDM at medium, long, and xlong gap settings, where the RMSE is reduced by 37%, 7%, and 8%, respectively. However, in the short gap setting, the RMSE of the IDM is 13% lower than that in the OVRV model.

As the value for RMSE in the medium setting simulation shows, the OVRV outperforms IDM by 37%. This difference in the performance can be observed in Fig. 7a between seconds 10 to 20, when the following vehicle is accelerating. The IDM simulated speed has a slight delay in accelerating in comparison to OVRV simulation and the experimental data. The effect of that can be observed in Fig. 7b when this delay in accelerating produces a large gap between the IDM simulated spacing and the experimental spacing between seconds 10 to 50. The nonlinear acceleration and deceleration described by IDM are out of place for EVs, which could yield constant power and braking regardless of the vehicle speed.

The RMSE value for the long gap setting shows that the performance of the OVRV is almost the same as the IDM. As Figure 8a demonstrates, the OVRV simulation has some small overshoots when the following vehicle is decelerating. In contrast, the IDM matches the EV-ACC vehicle speed observed in the experimental data. The effect of this behavior can be seen better in Figure 8b. When the vehicle is initially decelerating, the simulated OVRV spacing lags the experimental spacing. However, there is a gap between the IDM simulated spacing and the experimental spacing when the vehicle is accelerating between seconds 20 to 30.

Overall, the plots in Fig. 7 and 8 show that both models accurately capture the EV-ACC following dynamics. While

Gap setting	IDM							OVRV				
	v_0 (m/s)	τ (s)	s_0 (m)	δ -	α (m/s^2)	β (m/s^2)	RMSE (m)	k_1 (s^{-2})	k_2 (s^{-1})	τ (s)	η (m)	RMSE (m)
Short	33.37	1.56	2.04	3.99	2.06	9.00	1.06	0.06	0.35	1.00	9.66	1.23
Medium	33.34	1.63	2.02	4.02	2.01	8.97	1.46	0.08	0.54	1.03	11.88	1.06
Long	33.36	1.67	2.41	3.96	1.86	8.96	0.44	0.06	0.38	1.24	12.40	0.41
Xlong	33.30	2.17	5.23	3.66	1.65	8.98	0.51	0.05	0.39	1.53	15.00	0.47

TABLE I: Parameter values for different gap settings in IDM and OVRV.

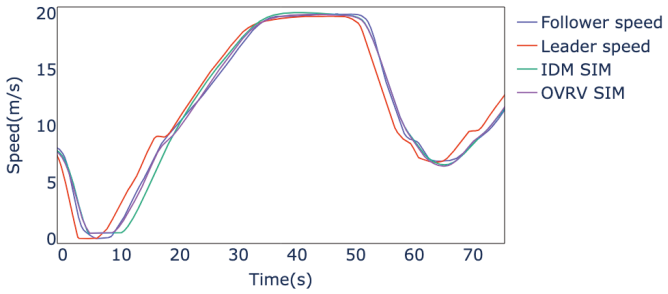

(a) The IDM and OVRV simulation on the velocity of the following vehicle for medium gap setting.

(b) The IDM and OVRV simulation on the spacing of the following vehicle for medium gap setting.

Fig. 7: Performance comparison of IDM and OVRV on the data of the medium gap setting.

(a) The IDM and OVRV simulation on the velocity of the following vehicle for long gap setting.

(b) The IDM and OVRV simulation on the spacing of the following vehicle for long gap setting.

Fig. 8: Performance comparison of IDM and OVRV on the data of the long gap setting.

the OVRV is slightly better at reproducing the spacing observed in the experiments, IDM appears to better match the lack of speed overshoot of the following vehicle. This suggests that further microscopic model development might be needed to accurately model EV-ACC vehicles.

B. Amplification analysis of a string of vehicles

To compare the performance of calibrated models EV-ACC vehicles with ICE-ACC vehicles, we conducted simulations of a string of 10 vehicles with a pre-defined velocity of the lead vehicle. For the EV-ACC vehicles, the model parameter values are short gap setting sets in Table I. For the ICE-ACC vehicles, the model parameter values are adopted from the short gap (minimum) setting in [23], where $\boldsymbol{\theta}_{\text{OVRV}} = [0.05, 0.26, 9.4, 0.58]^\top$ and $\boldsymbol{\theta}_{\text{IDM}} = [43.6, 1.0, 13.5, 8.0, 0.9, 9.0]^\top$, respectively. This simulation experiment will allow us to understand how EV-ACC vehicles might impact traffic flow, as compared to ICE-ACC vehicles.

Fig. 9 depicts the simulations of a string of EV-ACC vehicles and ICE-ACC vehicles with the OVRV model and the IDM, respectively. With the definition of string stability in mind, the increase of wave amplification implies more string instabilities. On the contrary, the dissipation of waves suggests less string instabilities. Specifically, when simulating the OVRV model for the EVs and the ICE vehicles in Figs. 9a and 9b, the reduction in wave amplification over the platoon of ICE-ACC vehicles is not as pronounced as EV-ACC vehicles.

Overshooting in the OVRV model may overestimate the amplification which suggests that further microscopic model development might be needed to fully capture the true amplification.

VI. Conclusions

This study employs widely used microscopic car-following models to describe the vehicle dynamics of EV-ACC vehicles. The model parameters are calibrated based on an experiment conducted with commercially available EV-ACC vehicles. While the calibration results show that the OVRV model outperforms the IDM in most of the gap settings indicating the OVRV can capture the driving behavior of EV-ACC vehicles, the IDM is better suited for describing the lack of following vehicle speed overshoot observed in the experimental data collected on EV-ACC vehicles. The results show that, while current models are capable of describing the dynamics of EV-ACC vehicles, new, high-fidelity models are needed to accurately describe all aspects of EV-ACC car following.

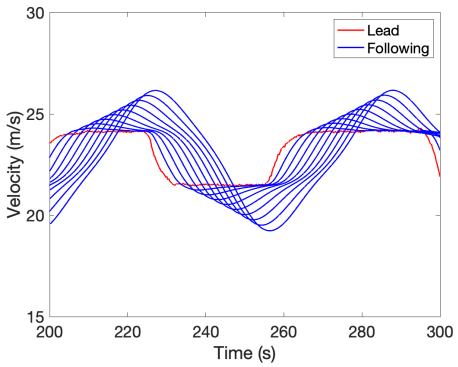

(a) Simulation of a string of EV-ACC vehicles using the OVRV model.

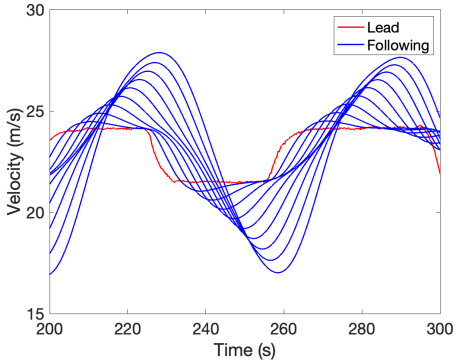

(b) Simulation of a string of ICE-ACC vehicles using the OVRV model.

Fig. 9: Simulation of a string of vehicles with the calibrated parameter values in Table I for EV-ACC vehicles and the model parameter values adopted from [23] for ICE-ACC vehicles. (a) and (b) are simulations with the OVRV model.

The calibration results provide valuable insights into the vehicle dynamics of EV-ACC vehicles. In future research, the study will focus on developing higher-fidelity microscopic car-following models for EV-ACC vehicles.

The preliminary results presented in this manuscript suggest that EV-ACC vehicles may reduce traffic wave amplification, which may result in an increase in traffic throughput. Follow-up work will investigate the impacts of EV-ACC vehicles on traffic flow in more detail. Furthermore, exploring the combined effects of human-driven vehicles, ICE-ACC vehicles, and EV-ACC vehicles in a mixed autonomy environment, which may become a reality in the near future, would be an interesting avenue to explore.

REFERENCES

[1] R. E. Stern, S. Cui, M. L. D. Monache, R. Bhadani, M. Bunting, M. Churchill, N. Hamilton, R. Haulcy, H. Pohlmann, F. Wu, B. Piccoli, B. Seibold, J. Sprinkle, and D. B. Work, "Dissipation of stop-and-go waves via control of autonomous vehicles: Field experiments," *Transportation Research Part C: Emerging Technologies*, vol. 89, pp. 205 – 221, 2018. [Online]. Available: http://www.sciencedirect.com/science/article/pii/S0968090X18301517

[2] A. Talebpour and H. S. Mahmassani, "Influence of connected and autonomous vehicles on traffic flow stability and throughput," *Transportation Research Part C: Emerging Technologies*, vol. 71, pp. 143–163, 2016.

[3] M. Shang and R. Stern, "Impacts of commercially available adaptive cruise control vehicles on highway stability and throughput," *Transportation Research Part C: Emerging Technologies*, vol. 122, p. 102897, 2021.

[4] L. C. Davis, "Effect of adaptive cruise control systems on traffic flow," *Physical Review E*, vol. 69, no. 6, p. 066110, 2004.

[5] Y. Qin, H. Wang, and B. Ran, "Stability analysis of connected and automated vehicles to reduce fuel consumption and emissions," *Journal of Transportation Engineering, Part A: Systems*, vol. 144, no. 11, p. 04018068, 2018.

[6] M. Aycin and R. Benekohal, "Comparison of car-following models for simulation," *Transportation research record*, vol. 1678, no. 1, pp. 116–127, 1999.

[7] D. C. Gazis, R. Herman, and R. B. Potts, "Car-following theory of steady-state traffic flow," *Operations Research*, vol. 7, no. 4, pp. 499–505, 1959.

[8] M. Bando, H. K., A. Nakayama, A. Shibata, and Y. Sugiyama, "Dynamical model of traffic congestion and numerical simulation," *Physical Review E*, vol. 51, no. 2, pp. 1035–1042, 1995.

[9] M. Treiber, A. Hennecke, and D. Helbing, "Congested traffic states in empirical observations and microscopic simulations," *Physical Review E*, vol. 62, no. 2, p. 1805, 2000.

[10] L. C. Davis, "The effects of mechanical response on the dynamics and string stability of a platoon of adaptive cruise control vehicles," *Physica A: Statistical Mechanics and its Applications*, vol. 392, no. 17, pp. 3798–3805, 2013.

[11] G. Gunter, D. Gloudemans, R. Stern *et al.*, "Are commercially implemented adaptive cruise control systems string stable?" *IEEE Transactions on Intelligent Transportation Systems*, vol. 22, no. 11, pp. 6992–7003, 2020.

[12] G. Gunter, R. Stern, and D. Work, "Modeling adaptive cruise control vehicles from experimental data: model comparison," in *2019 IEEE Intelligent Transportation Systems Conference (ITSC)*. IEEE, 2019, pp. 3049–3054.

[13] V. Milanés, S. E. Shladover, J. Spring *et al.*, "Cooperative adaptive cruise control in real traffic situations," *IEEE Transactions on Intelligent Transportation Systems*, vol. 15, no. 1, pp. 296–305, 2014.

[14] M. Shang, B. Rosenblad, and R. Stern, "A novel asymmetric car following model for driver-assist enabled vehicle dynamics," *IEEE Transactions on Intelligent Transportation Systems*, 2022.

[15] P. C. Kan-Munoz, S. Lapardhaja, and X. D. Kan, "Field experiments of commercially available automated vehicles on freeways," Tech. Rep., 2021.

[16] C. Lee, T. Majumder, K. Yagantekin, X. Kan, and M. Yang, "Field experiment on the capacity impact of vehicle automation on electric vehicles (evs) – case study of adaptive cruise control (ACC)," in *Transportation Research Board Annual Meeting*. TRB, 2023, pp. 23–04 398.

[17] D. Gazis, R. Herman, and R. Rothery, "Nonlinear follow-the-leader models of traffic flow," *Operations research*, vol. 9, no. 4, pp. 545–567, 1961.

[18] J. Olstam and A. Tapani, *Comparison of Car-following models*. Swedish National Road and Transport Research Institute Linköping, 2004, vol. 960.

[19] R. Rajamani, *Vehicle dynamics and control*. Springer Science & Business Media, 2011.

[20] P. Ioannou and C. Chien, "Autonomous intelligent cruise control," *IEEE Transactions on Vehicular Technology*, vol. 42, no. 4, pp. 657–672, 1993.

[21] V. Milanés and S. E. Shladover, "Modeling cooperative and autonomous adaptive cruise control dynamic responses using experimental data," *Transportation Research Part C: Emerging Technologies*, vol. 48, pp. 285–300, 2014.

[22] G. Gunter, C. Janssen, W. Barbour, R. Stern, and D. Work, "Model based string stability of adaptive cruise control systems using field data," *IEEE Transactions on Intelligent Vehicles*, vol. 5, no. 1, pp. 90–99, 2019.

[23] F. De Souza and R. E. Stern, "Calibrating microscopic model for commercially available autonomous driving systems: a multi-objective approach," in *Transportation Research Board Annual Meeting*, 2019.

[24] Y. Wang, G. Gunter, M. Nice, M. Delle Monache, and D. Work, "Online parameter estimation methods for adaptive cruise control systems," *IEEE Transactions on Intelligent Vehicles*, vol. 6, no. 2, pp. 288–298, 2020.